Title: A subset of CD4+ effector memory T cells limit immunity to pulmonary viral infection and prevent tissue pathology via activation of latent TGFβ

McEntee CP[1,2,3*], Houston S[1,2,3], Finlay CM[1,2,3#], Rossi S[1,2,3], Liu G[4], Shaw TN[1,3†], Casulli J[1,2,3], Fife M[1,3], Smedley C[1,2,3], Griffith TS[5], Pepper M[6], Hussell T[1,3], Hansbro PM[4], Schwartz J-M[7], Paidassi H[8], Travis MA[1,2,3]

1. Lydia Becker Institute for Immunology and Inflammation,

2. Wellcome Trust Centre for Cell-Matrix Research,

3. Division of Immunology, Immunity to Infection and Respiratory Medicine, Faculty of Biology, Medicine and Health, Manchester Academic Health Sciences Centre, University of Manchester, UK.

4. Centre for Inflammation, Centenary Institute and University of Technology Sydney, Faculty of Science, School of Life Sciences, Sydney, New South Wales, Australia.

5. University of Minnesota, Department of Urology, Center for Immunology, Minneapolis, MN, USA.

6. Department of Immunology, University of Washington School of Medicine, Seattle, WA, USA.

7. School of Biological Sciences, Faculty of Biology, Medicine and Health, University of Manchester, UK.

8. CIRI, Centre International de Recherche en Infectiologie, 'Normal and Pathogenic B cells' Team, Univ Lyon, Inserm U1111, Université Claude Bernard Lyon 1, CNRS UMR5308, ENS de Lyon, F-69007 Lyon France.

[*]Current address: School of Biochemistry and Immunology, Trinity Biomedical Sciences Institute, Trinity College Dublin, Dublin 2, Ireland

[#]Current address (Conor): Trinity Translational Medicine Institute, Trinity College Dublin, Dublin 2, Ireland

[†]Current address: Institute of Immunology and Infection Research, School of Biological Sciences, University of Edinburgh, Edinburgh, United Kingdom

Corresponding author: Mark A. Travis, 2.14b Core Technology Facility, Faculty of Biology, Medicine and Health, University of Manchester, Grafton Street, Manchester, M13 9NT, UK.

E-mail: mark.travis@manchester.ac.uk Tel: +44 161 275 1701

Abstract

A rapid immune response to pathogen re-exposure underpins immunological memory, with protection against divergent pathogens such as heterologous or novel viral strains requiring cross-reactive memory T cells. Understanding the pathways that control memory T cell function is therefore important for the rational design of viral vaccines and will aid the discovery of therapies to boost anti-viral immunity. Here, we identify a sub-population of memory T cells that limit secondary immune responses to viral re-infection, which is crucial in preventing host tissue damage. We show that a population of $CD4^+$ effector memory T (T_{EM}) cells activate the important immunoregulatory cytokine TGFβ, via expression of an integrin, αvβ8. Integrin αvβ8 expression marks a transcriptionally distinct sub-population of $CD4^+$ T_{EM}, enriched for anti-inflammatory pathways. Loss of integrin αvβ8 on murine $CD4^+$ T_{EM}, but not $Foxp3^+$ regulatory T cells (T_{REG}), led to exacerbated virus-specific $CD8^+$ T cell responses following secondary influenza A virus (IAV) infection, which was associated with enhanced viral clearance. However, although accelerating clearance, loss of integrin αvβ8 expression on $CD4^+$ T_{EM} resulted in enhanced lung pathology following secondary IAV infection, which was completely reversed by adoptive transfer of $αvβ8^+$ $CD4^+$ T_{EM} cells. These data highlight a new pathway by which a distinct $CD4^+$ memory T cell subset restrains anti-viral immunity to prevent host tissue damage during secondary viral infection. Such pathways could be targeted therapeutically to either boost memory T-cell-mediated immunity or restrain host tissue damage during viral infection.

72 **Main text**

73 Whether induced by natural infection or vaccination, the development of robust
74 immunological memory is a cornerstone of sustained protective immunity against viruses,
75 either by directly targeting infected cells for killing or through the induction of high affinity,
76 virus-specific antibody responses. While viral surface proteins, the primary targets for
77 antibodies, can accumulate mutations over time leading to reduced antibody binding affinity
78 and neutralising efficacy, memory T cells typically recognise conserved epitopes which are
79 often shared between different viral strains or variants. Thus, virus-specific memory T cells
80 exhibit cross-reactivity to heterologous viruses, referred to as heterosubtypic immunity, and
81 are therefore a key component of long-lasting immunological memory, particularly as viral
82 variants emerge over time[1,2]. While the differentiation and maintenance of memory T cells is
83 highly dynamic, and functional/phenotypic plasticity between subsets has been reported[3,4],
84 traditionally they have been subdivided into three major subsets based on their expression of
85 homing markers and anatomical location. Circulating $CD44^{high}$ memory T cells can be stratified
86 into central or effector memory T cells (T_{CM} or T_{EM} respectively) based on the expression or
87 absence of markers including CD62L (L-selectin) and CCR7 (C-C Motif Chemokine Receptor
88 7)[5]. $CD62L^{+}$ $CCR7^{+}$ T_{CM} migrate between the circulation and secondary lymphoid structures
89 whereas $CD62L^{-}$ $CCR7^{-}$ T_{EM} traffic between lymphoid and peripheral tissues. In contrast, the
90 third major memory T cell subset reside predominantly in non-lymphoid peripheral tissues
91 including the gastrointestinal tract, skin and lung and are referred to as tissue-resident
92 memory T cells (T_{RM})[6], although recent data do suggest that T_{RM} populations can also leave
93 the tissue and circulate[7]. Given their importance in sustained, cross-reactive protective
94 immunity against common pathogens, understanding how memory T cells function is of

95 fundamental importance, not only to aide rational vaccine design, but also to identify
96 targetable pathways for anti-viral immunotherapies.
97
98 Here we show that a sub-population of $CD4^+$ T_{EM} control secondary immune responses to
99 respiratory viral infection by restraining the host T cell response. These cells are specialised
100 to activate the key immunoregulatory cytokine transforming growth factor-β (TGFβ) via
101 expression of the integrin αvβ8, exhibit an immune suppressive transcriptional profile, and
102 limit the frequency and cytotoxic potential of IAV-specific $CD8^+$ effector T cells during a
103 memory recall response. $CD4^+$ T_{EM} expressing integrin αvβ8 directly suppress $CD8^+$ T cells in a
104 TGFβ-dependent manner and are vital in preventing tissue pathology during secondary
105 infection. Additionally, we find that integrin αvβ8 is expressed by human $CD4^+$ T_{EM}, but no
106 other memory or naïve human $CD4^+$ or $CD8^+$ T cells, highlighting the potential of targeting this
107 pathway clinically to boost cytotoxic $CD8^+$ T cell responses in the context of anti-viral or cancer
108 immunotherapy. Together, our study uncovers a new suppressive role for a sub-population
109 of $CD4^+$ T_{EM} which express integrin αvβ8 and can activate latent TGFβ. These properties make
110 integrin $αvβ8^+$ $CD4^+$ T_{EM} key regulators of anti-viral memory T cell responses and function to
111 prevent inflammation-induced pathology following respiratory viral infection.
112

113 **CD4$^+$ T$_{EM}$ express *Itgb8* and activate latent TGFβ.**

114 A crucial cytokine in the regulation of many different immune cells, especially T cells, is TGFβ[8].
115 TGFβ is initially secreted as a latent pro-form, consisting of the active moiety bound non-
116 covalently and encased by latency associated peptide (LAP), from which the active cytokine
117 must be liberated to function[9]. However, the role of TGFβ and its activation in controlling the
118 function of memory T cell responses is poorly understood.

119

120 To investigate whether TGFβ activation may play a role in regulating memory T cell function,
121 we first determined whether any memory T cell populations have the potential to activate
122 TGFβ. To this end, we assessed the expression of integrin αvβ8 on memory T cell subsets, a
123 molecule we and others have previously shown facilitates the activation of latent TGFβ by
124 immune cells[10]. To this end, we sorted multiple CD4$^+$ and CD8$^+$ splenic T cell populations from
125 Foxp3-YFP reporter mice[11] to assess expression of the gene encoding the integrin β8 subunit
126 (*Itgb8*) across several subsets by qRT-PCR (gating strategy shown in Figure S1a). As the
127 integrin β8 subunit uniquely pairs with the αv subunit, this approach enabled us to determine
128 relative expression of integrin αvβ8. Interestingly, in addition to the expected high levels of
129 expression of *Itgb8* by CD4$^+$ Foxp3$^+$ T$_{REG}$[12], we also found for the first time that CD4$^+$ T$_{EM}$
130 (CD44^{hi} CD62L$^-$) also expressed high levels of the gene (Figure 1a). In contrast, *Itgb8* was not
131 detected in naïve CD4$^+$ T cells (CD44^{lo} CD62L$^+$) nor CD4$^+$ T$_{CM}$ (CD44^{hi} CD62L$^+$). Similarly, all CD8$^+$
132 T cell subsets lacked expression of *Itgb8* (Figure 1a).

133

134 Next, to assess the expression of *Itgb8* at the single cell level, we utilised a novel dual reporter
135 mouse expressing GFP and tdTomato under control of the *Foxp3* and *Itgb8* promoters
136 respectively[13] (hereafter referred to as *Itgb8* reporter mice). We observed expression of *Itgb8*

137 in a subset of CD4$^+$ $T_{EM,}$ accounting for ~30% of the total CD4$^+$ T_{EM} pool (Figure 1b-c). In
138 contrast, no expression was detected in CD4$^+$ naïve or T_{CM} cells, or any CD8$^+$ T cell subsets
139 (Figure 1b-c), consistent with our qRT-PCR data (Figure 1a). Additionally, we also observed
140 the presence of *Itgb8*-expressing CD4$^+$ T_{EM} at other anatomical locations, including within
141 non-lymphoid tissues such as the lung (Figure S1b-c) and intestine (Figure S1d-e). Thus, the
142 expression of *Itgb8* is unique to CD4$^+$ T_{EM} amongst the circulating memory T cell pool.
143
144 Having determined that CD4$^+$ T_{EM} express *Itgb8*, we next investigated whether this enabled
145 these cells to activate latent TGFβ. To test this, we isolated CD4$^+$ T_{EM} from mice lacking *Itgb8*
146 expression on T cells (*Itgb8*$^{flox/flox}$ x CD4-Cre, hereafter called *Itgb8*$^{\Delta CD4}$ mice[14]) or their
147 littermate controls, and co-cultured them with an active TGFβ reporter cell line as previously
148 described[12]. We observed that CD4$^+$ T_{EM} activated latent TGFβ to levels comparable with CD4$^+$
149 Foxp3$^+$ T_{REG} (Figure 1d). This ability to activate latent TGFβ was entirely dependent on integrin
150 αvβ8, as TGFβ activation was completely abrogated in CD4$^+$ T_{EM} cells isolated from *Itgb8*$^{\Delta CD4}$
151 mice (Figure 1d). Taken together, these data show for the first time that CD4$^+$ T_{EM} uniquely
152 express *Itgb8* amongst the circulating memory T cell pool and can activate latent TGFβ in an
153 integrin αvβ8-dependent manner.
154
155 ***Itgb8*$^+$ CD4$^+$ T_{EM} exhibit a transcriptional profile associated with immune suppression.**
156 Although CD4$^+$ T_{EM} express *Itgb8* and can activate latent TGFβ, it is noteworthy that *Itgb8*
157 expression was not ubiquitous but rather restricted to a sub-population of CD4$^+$ T_{EM} (Figure
158 1b-c). These data could indicate stochastic expression within the population, or that
159 expression of *Itgb8* by CD4$^+$ T_{EM} is linked to a distinct phenotype or function compared to their
160 *Itgb8*-negative (*Itgb8*$^-$) counterparts. To investigate further, we purified *Itgb8*$^+$ and *Itgb8*$^-$ CD4$^+$

161 T_{EM} from *Itgb8* reporter mice and performed bulk RNA-seq to directly compare the
162 transcriptome of the two populations. We found that the two populations showed a
163 profoundly different transcriptional profile, with 1599 significantly differentially expressed
164 protein coding genes (DEGs) between *Itgb8*$^+$ and *Itgb8*$^-$ CD4$^+$ T_{EM} with a Log_2 fold change
165 greater than 0.5 (Figure 1e, Figure S2a-b, and Table S1). Amongst these DEGs were a number
166 of genes known to be associated with immune suppression or regulatory function, including
167 *Lag3*, *Tigit*, *Il10, Rnf128* and *Pdcd1*, which showed increased expression in *Itgb8*$^+$ T_{EM} relative
168 to the *Itgb8*$^-$ subset (Figure 1f). These data suggest *Itgb8*$^+$ CD4$^+$ T_{EM} may represent a
169 suppressive population of memory T cells. Such a function would fit with previous findings
170 demonstrating that other immune cells capable of activating TGFβ via integrin αvβ8, including
171 dendritic cells (DCs)[14-18] , T_{REGS}[12] and monocytes and macrophages[19], are associated with
172 immune suppressive or regulatory functions.
173
174 When sorting *Itgb8*$^+$ and *Itgb8*$^-$ CD4$^+$ T_{EM} from *Itgb8* reporter mice for RNA-seq analysis, Foxp3$^+$
175 T_{REGS} were excluded based on their expression of GFP. However, as several of the genes found
176 to be up-regulated in *Itgb8*$^+$ CD4$^+$ T_{EM} are also associated with regulatory immune responses,
177 we performed a four-way bulk RNA-seq experiment to directly address whether *Itgb8*$^+$ Foxp3$^-$
178 CD4$^+$ T_{EM} were transcriptionally similar to CD4$^+$ Foxp3$^+$ T_{REG}. Principle component analysis
179 (PCA) revealed each of the four CD4$^+$ T cell subsets to be transcriptionally distinct from one
180 another (Figure 1g and Table S2). Unexpectedly, we observed more variance based on *Itgb8*
181 expression status (60%) than the difference between T_{EM} and T_{REG} (Foxp3$^-$ and Foxp3$^+$; 30%)
182 (Figure 1g), a feature confirmed by correlating gene expression across groups (Figure S2c).
183 Notably, expression of specific suppressive genes was enriched in both *Itgb8*$^+$ Foxp3$^-$ T_{EM} and
184 *Itgb8*$^+$ Foxp3$^+$ T_{REG} relative to each of their respective *Itgb8*$^-$ counterparts (Figure 1h).

185 However, although sharing some suppression-related gene expression, there were clear
186 differences in expression of other T cell-associated genes (Figure S2d). Thus, these data show
187 *Itgb8*$^{+}$ Foxp3^{-} T_{EM} are transcriptionally distinct from *Itgb8*$^{+}$ Foxp3^{+} T_{REG} and identifies a Foxp3^{-}
188 memory T cell subset with an immune-suppressive transcriptional profile.
189
190 **_Itgb8_$^{+}$ CD4^{+} T_{EM} suppress IAV-specific CD8^{+} memory T cell responses.**
191 Next, we sought to determine the functional importance of *Itgb8* expression by CD4^{+} T_{EM} *in*
192 *vivo*, in the context of an antigen-specific recall response following secondary infection. To
193 this end, we utilised the well-characterised secondary influenza challenge model using
194 heterologous strains of IAV. Briefly, *Itgb8*$^{\Delta CD4}$ and littermate control mice were infected
195 intranasally with the IAV strain X31 (H3N2), allowed to recover for ~6 weeks, and then re-
196 challenged with the IAV strain A/PR/8 (H1N1, PR8) (Figure 2a). The magnitude of the anti-viral
197 T cell responses was tracked using major histocompatibility complex (MHC) class I- and class
198 II-restricted tetramers, which facilitated identification of IAV nucleoprotein (NP)-specific CD8^{+}
199 and CD4^{+} T cell responses, respectively (representative gating strategy shown in Figure S3a).
200 We found that, in comparison to littermate controls, by day 8 post-infection *Itgb8*$^{\Delta CD4}$ mice
201 had significantly enhanced IAV-specific CD8^{+} T cell responses in the lung following re-
202 challenge with PR8, both in terms of frequency (Figure 2b-c) and absolute cell numbers
203 (Figure 2d), with similar increases observed in the lung-draining lymph nodes (Figure S3b-c).
204 In contrast, IAV-specific CD4^{+} T cell responses were unaffected (Figure S3d-e). Notably, no
205 differences in the abundance of IAV-specific CD8^{+} T cells were observed following primary
206 infection (Figure S3f-g), indicating *Itgb8* serves to restrain cytotoxic T lymphocyte (CTL)
207 responses following reactivation, rather than regulating their differentiation following
208 primary infection.

209 As both Foxp3$^+$ T_{REG} and CD4$^+$ T_{EM} express *Itgb8* (Figure 1a-c and [12]), a caveat of the
210 experiments using *Itgb8*$^{\Delta CD4}$ mice is that expression of the integrin is ablated on both T cell
211 subsets. Crucially however, the hyper-responsive IAV-specific CD8$^+$ T cell phenotype we
212 observed following secondary IAV infection of *Itgb8*$^{\Delta CD4}$ mice is not due to a lack of *Itgb8*
213 expression in CD4$^+$ T_{REG}, as deletion of *Itgb8* expression exclusively on Foxp3$^+$ T_{REG} (*Itgb8*$^{flox/flox}$
214 x Foxp3-Cre[12], herein called *Itgb8*$^{\Delta Foxp3}$ mice) exhibited no such phenotype after IAV re-
215 infection (Figure S3h-i).
216
217 Next, we analysed the effector profile of IAV-specific CD8$^+$ T cells in *Itgb8*$^{\Delta CD4}$ mice following
218 secondary influenza challenge. In addition to being more abundant after secondary infection,
219 IAV-specific CD8$^+$ T cells from *Itgb8*$^{\Delta CD4}$ mice exhibited heightened effector properties,
220 including enhanced production of granzyme B in the lung (Figure 2e-g) and lung-draining LN
221 (Figure S3j-k) and increased expression of genes encoding molecules associated with
222 cytotoxic T cell responses such as granzyme A (*Gzma*), granzyme B (*Gzmb*), perforin (*Prf1*) and
223 interferon gamma (*Ifng*) (Figure 2h-k).
224
225 Additionally, recent evidence suggests TGFβ is crucial in the formation of CD8$^+$ T_{RM}, and that
226 activation of TGFβ by DCs and epithelial cells in an αv integrin-dependent manner promotes
227 the formation of T_{RM} at barrier sites such as the skin and intestine[20-22]. However, when we
228 analysed the development of IAV-specific CD8$^+$ T_{RM} in the lung following secondary infection
229 (see materials and methods, and Figure S3a for gating strategy), this remained intact, and was
230 even elevated, in *Itgb8*$^{\Delta CD4}$ mice (Figure S3l).
231

232 Thus, taken together, these data suggest *Itgb8*$^{+}$ CD4^{+} T_{EM} have a suppressive phenotype and
233 dampen CD8^{+} T cell numbers and effector function *in vivo* during secondary viral infection.
234 Additionally, this cellular pathway of TGFβ activation is not involved in induction of CD8^{+} T_{RM}
235 in the lung, pointing to a dichotomy in functional outcomes depending on the cell type
236 responsible for the activation of TGFβ.
237
238 ***Itgb8*$^{+}$ CD4^{+} T_{EM} directly suppress Influenza virus-specific CD8^{+} memory T cell responses via**
239 **activation of TGFβ.**
240 Thus far, we have shown that deletion of *Itgb8* on T cells in *Itgb8*$^{\Delta CD4}$ mice results in enhanced
241 CD8^{+} T cell responses during secondary IAV infection. Furthermore, T cell expression of *Itgb8*
242 appears to be limited to CD4^{+} T_{EM} and CD4^{+} Foxp3^{+} T_{REG} (Figure 1a-c and [12]), and mice lacking
243 expression of *Itgb8* on Foxp3^{+} T_{REG} do not show any phenotype during secondary IAV infection
244 (Figure S3h-i). This strongly suggests that the enhanced IAV-specific CD8^{+} T cell responses
245 observed in *Itgb8*$^{\Delta CD4}$ mice is due to lack of *Itgb8* expression by CD4^{+} T_{EM}. To prove this
246 unequivocally and directly test the suppressive capacity of *Itgb8*$^{+}$ CD4^{+} T_{EM} *in vivo*, we
247 designed an experiment to assess whether *Itgb8*$^{+}$ CD4^{+} T_{EM} were sufficient to reverse the
248 enhanced IAV-specific CD8^{+} T cell responses in *Itgb8*$^{\Delta CD4}$ mice following secondary IAV
249 infection. To this end, we isolated *Itgb8*$^{+}$ and *Itgb8*$^{-}$ CD4^{+} T_{EM} from *Itgb8*-reporter mice
250 following resolution of primary X31 infection and adoptively transferred them into
251 convalescent *Itgb8*$^{\Delta CD4}$ mice prior to secondary PR8 infection (Figure 3a). We found that
252 although transfer of *Itgb8*$^{-}$ CD4^{+} T_{EM} had no effect, transfer of *Itgb8*$^{+}$ CD4^{+} T_{EM} completely
253 reversed the enhanced NP-specific CD8^{+} T cell response to IAV re-challenge seen in *Itgb8*$^{\Delta CD4}$
254 mice, to levels observed in littermate controls (Figure 3b-c). In addition, such an effect was
255 not limited to NP-specific CD8^{+} T cells, as transfer of *Itgb8*$^{+}$ CD4^{+} T_{EM} also efficiently attenuated

256 IAV polymerase (PA)-specific CD8$^+$ T cell responses in *Itgb8*$^{\Delta CD4}$ recipient mice to levels seen
257 in littermate controls, whereas transfer of *Itgb8*$^-$ CD4$^+$ T_{EM} had no such effect (Figure S4a-b).
258 Thus, these data show that *Itgb8*$^+$ CD4$^+$ T_{EM} cause suppressive effects *in vivo* and are sufficient
259 to reverse enhanced IAV-specific CD8$^+$ T cell responses in *Itgb8*$^{\Delta CD4}$ mice.
260
261 In light of these findings, we next sought to elucidate the mechanism(s) by which *Itgb8*$^+$ CD4$^+$
262 T_{EM} can suppress CD8$^+$ T cell responses after viral re-infection. As expression of *Itgb8* by CD4$^+$
263 T_{EM} enables them to activate TGFβ (Figure 1d), and TGFβ can directly inhibit CD8$^+$ T cells[23], we
264 postulated that *Itgb8*$^+$ CD4$^+$ T_{EM} could directly suppress CD8$^+$ T cell responses via their ability
265 to activate TGFβ. To investigate this hypothesis, we performed an *ex vivo* CD8$^+$ T cell
266 proliferation assay and tested the ability of *Itgb8*$^+$ and *Itgb8*$^-$ CD4$^+$ T_{EM} to modulate the
267 proliferative response. To this end, we isolated *Itgb8*$^+$ and *Itgb8*$^-$ CD4$^+$ T_{EM} from *Itgb8* reporter
268 mice and co-cultured each of these subsets separately with Cell Trace Violet (CTV)-labelled
269 CD8$^+$ T cells that were activated with anti-CD3ξ and anti-CD28 antibodies. We found that CD8$^+$
270 T cell proliferation was significantly inhibited when responder cells were co-cultured with
271 *Itgb8*$^+$, but not *Itgb8*$^-$ CD4$^+$ T_{EM} (Figure 3d-e). Furthermore, the inhibition of CD8$^+$ T cell
272 proliferation by *Itgb8*$^+$ CD4$^+$ T_{EM} was wholly dependent on active TGFβ, as this inhibition was
273 completely reversed when the cells were co-cultured in the presence of a TGFβ blocking
274 antibody (Figure 3d-e). Moreover, addition of exogenous, active TGFβ to co-cultures of *Itgb8*$^-$
275 CD4$^+$ T_{EM} with CD8$^+$ responders also significantly reduced CD8$^+$ T cell proliferation (Figure 3f-
276 g), further implicating TGFβ as a key factor involved in immune suppression mediated by
277 *Itgb8*$^+$ CD4$^+$ T_{EM}.

278 Taken together, these data show that *Itgb8*$^{+}$ CD4^{+} T_{EM} restrain IAV-specific CD8^{+} T cells *in vivo*,
279 a function facilitated via their ability to activate TGFβ in an integrin αvβ8-dependent manner,
280 which can act directly on CD8^{+} T cells to inhibit their proliferation.
281
282 ***Itgb8*$^{+}$ CD4^{+} T_{EM} slow viral clearance but are vital in preventing lung pathology following**
283 **viral re-infection.**
284 We next sought to determine the physiological relevance of *Itgb8*$^{+}$ CD4^{+} T_{EM}–mediated
285 control of anti-viral memory T cell responses. To this end, we first analysed the ability of
286 *Itgb8*$^{\Delta CD4}$ mice and their littermate controls to clear the virus after secondary IAV infection.
287 We found that *Itgb8*$^{\Delta CD4}$ mice showed significantly more robust expulsion of the virus, with
288 reduced copies of viral RNA detected at days 5 and 8 post-secondary infection compared to
289 littermate controls (Figure 4a). In contrast, we did not observe any difference in the ability of
290 *Itgb8*$^{\Delta Foxp3}$ mice to clear viral load after secondary infection compared to littermate controls
291 (Figure S5a), providing strong evidence that the lack of *Itgb8* expression on Foxp3^{+} T_{REG} is not
292 responsible for the enhanced viral clearance in *Itgb8*$^{\Delta CD4}$ mice. Taken together, our data
293 indicate that *Itgb8*$^{+}$ CD4^{+} T_{EM}-mediated restraint of CD8^{+} T cells during secondary IAV infection
294 limits the ability of mice to rapidly clear the virus.
295
296 Our studies demonstrated a novel role for *Itgb8*-expressing CD4^{+} T_{EM} in restraining anti-viral
297 CTL responses and slowing clearance of the virus. We next wanted to determine the
298 functional importance of a pathway that essentially limits host immunity to pathogenic
299 challenge. Based on the potent cytotoxic profile of IAV-specific CD8^{+} T cells in *Itgb8*$^{\Delta CD4}$ mice
300 (Figure 2e-k), we hypothesised that this pathway may be important in limiting infection-
301 induced inflammation and lung pathology. Indeed, *Itgb8*$^{\Delta CD4}$ mice exhibited significantly

302 enhanced lung inflammation compared to littermate control animals after secondary
303 infection, with inflammatory cells locating around airways and blood vessels and infiltrating
304 the parenchymal area (Figure 4b-c). There was no difference in lung pathology between
305 *Itgb8*$^{\Delta CD4}$ mice and littermate controls after primary IAV infection (Figure S5b-c), again
306 indicating a role for *Itgb8*$^{+}$ CD4^{+} T_{EM} in controlling T cell responses during re-infection rather
307 than primary infection.
308
309 We next determined whether enhanced pathology observed after secondary IAV infection in
310 *Itgb8*$^{\Delta CD4}$ mice was directly due to the absence of *Itgb8*$^{+}$ CD4^{+} T_{EM}. To this end, we analysed
311 lung pathology following secondary IAV infection of *Itgb8*$^{\Delta CD4}$ mice that received either *Itgb8*$^{+}$
312 or *Itgb8*$^{-}$ CD4^{+} T_{EM}. Transfer of *Itgb8*$^{+}$ CD4^{+} T_{EM}, but not *Itgb8*$^{-}$ CD4^{+} T_{EM}, completely reversed
313 the enhanced lung pathology seen in *Itgb8*$^{\Delta CD4}$ mice after secondary infection (Figure 4d-e),
314 restoring histology and inflammation scores to that seen in control mice (Figure 4b-c). Taken
315 together, these data strongly indicate that although *Itgb8*$^{+}$ CD4^{+} T_{EM} slow the ability of the
316 host to clear viral load, they are essential in restraining pathogenic anti-viral CD8^{+} T cell
317 responses to prevent tissue pathology following re-infection.
318
319 Having discovered that integrin αvβ8 expression identifies a sub-population of immune
320 suppressive murine CD4^{+} T_{EM}, which can restrain effector recall responses and prevent overt
321 inflammatory sequelae, we sought to determine whether a similar population might be
322 present in humans. To test this, we isolated human peripheral blood mononuclear cells
323 (PBMCs) and assessed expression of integrin αvβ8 on human T cell subsets by flow cytometry
324 using a monoclonal antibody specific for human αvβ8[15] (gating strategy shown in Figure S6).

325 In agreement with our pre-clinical data, expression of integrin αvβ8 was restricted primarily
326 to $CD4^+$ T_{EM} in human PBMCs (Figure 4f-g).
327
328 Together, our data for the first time show that a subset of cells classed as $CD4^+$ memory T cells
329 can be suppressive during re-infection. This suppressive function is reliant on their expression
330 of an integrin, αvβ8, which enables them to activate TGFβ. We find that these cells are crucial
331 in restraining $CD8^+$ T cell responses during re-infection with IAV in the lung but are also
332 present in the intestine. Thus, important future work will determine if these cells have a
333 broader function in regulating secondary immunity in other organs to a wide range of
334 challenges, or if the cells are specific to pulmonary immunity.
335
336 Our findings have important implications to how the immune system balances responses to
337 re-infection. Although immunological memory has evolved to promote more robust
338 responses to subsequent infections, it now appears that memory T cell subsets can also limit
339 the robustness of this response. In situations where re-infection is proving hard to irradicate,
340 it could be beneficial to inhibit the function of these suppressive memory T cells, via blocking
341 integrin αvβ8 and therefore the ability of these cells to activate TGFβ, to boost $CD8^+$ T cell
342 responses.
343
344 However, caution would be required with any such approaches, as these suppressive memory
345 T cells appear critical in limiting host pathology during re-infection. Thus, strategies would
346 have to balance the beneficial effects of promoting immunity to re-infection, with potential
347 tissue damage associated with an exacerbated response. A phase I clinical trial is already
348 underway in cancer using an antagonist of integrin αvβ8 to block TGFβ activation, based on

successful pre-clinical studies[24-26]. Based on our findings that this molecular pathway is important in limiting tissue pathology to re-infection, attention to the infection status of the patients during treatment periods may be prudent.

355 **Materials and methods**

356

357 ***Mice***

358 Conditional deletion of *Itgb8* (β8 integrin) expression specifically in T cells or T_{REG} was
359 achieved by crossing mice with a conditional floxed allele of *Itgb8* with CD4-Cre[14] or Foxp3-
360 YFP-Cre[12] mice. All mice were used for experiments at 8 to 12 weeks of age, with littermates
361 used as control. *Itgb8*-IRES-TdTomato mice, generated as previously described[13], were
362 provided by Dr. H. Paidassi and bred at the University of Manchester. All experiments were
363 approved under a project license granted by the Home Office UK, reviewed by the University
364 of Manchester Animal Welfare and Ethical Review Body and were performed in accordance
365 with the UK Animals (Scientific Procedures) Act of 1986. Mice were bred and maintained in
366 specific pathogen–free conditions at Bio Safety Level 2 with a 12-hour light/dark cycle and
367 food and water *ab libitum*.

368

369 ***Influenza A Virus Infections***

370 *Itgb8* conditional knockout mice and their littermate controls were anaesthetised with 2.5%
371 inhalable isoflurane and inoculated with 10^3 PFU of the IAV strain X31 (H3N2) or 10^1 PFU of
372 the IAV strain A/PR/8 (H1N1, PR8) intranasally, resulting in a transient infection and mild to
373 moderate weight loss. For secondary IAV challenge studies mice were inoculated with 10^3
374 PFU IAV-X31 and subsequently re-challenged ~6 weeks later with 10^1 PFU of the heterologous
375 strain IAV-PR8 and immune responses assessed at time-points indicated in the figure legends.

376

377

378 ***Lung digest***

379 Lungs were transferred into 7 ml bijoux tubes containing 500 µl digestion mix consisting of 5
380 mg/ml collagenase I (Gibco) and 10 µg/ml DNase I (Sigma) in RPMI and finely minced with
381 scissors. An additional 1.5 ml of digestion mix was then added to samples and incubated in a
382 shaking incubator at 37°C for 40 minutes. Enzymes were quenched with ice-cold 10% RPMI
383 medium containing 10% FCS, and cells pelleted via centrifugation at 400 x g for 8 minutes.
384 Cell pellets were re-suspended in 2 ml red blood cell lysis buffer (Sigma) and washed with ice-
385 cold 10% FCS in RPMI prior to staining for flow cytometry.

386

387 ***Flow Cytometry***

388 Cell suspensions were transferred into 5 ml round bottom polystyrene tubes, washed in PBS
389 and stained with fixable viability Zombie dyes (Biolegend) diluted in PBS. Staining was
390 quenched by washing in FACS buffer (PBS with 2 mM EDTA and 2% FCS) after which cells were
391 incubated with anti-CD16/32 (Fc block, clone 2.4G2, BD Biosciences) for 15 minutes at 4°C to
392 prevent non-specific binding. Without washing, antibodies specific for surface markers were
393 diluted in FACS buffer and added 1:1 directly onto samples and incubated for a further 20
394 minutes at 4°C protected from light. Stained samples were then washed in PBS and either re-
395 suspended in FACS buffer for immediate sorting on a BD FACSAria™ cell sorter or fixed using
396 eBioscience™ Foxp3 / Transcription Factor Staining Buffer Set as per manufacturer's
397 guidelines. For experiments requiring T cell sorting, single cell suspensions underwent a
398 negative selection pre-enrichment using EasySep™ pan-T cell or memory $CD4^+$ T cell isolation
399 kits as per manufacturer's guidelines (Stemcell™ Technologies).

400

401 To stain for intracellular markers or cytokines, fixed/permeabilsed samples were incubated
402 with antibodies diluted in 1X permeabilisation buffer. Samples were washed twice and re-
403 suspended in FACS-EDTA prior to acquisition on a BD LSR Fortessa™ or BD Symphony™.
404 Antibodies used for flow cytometry and FACS were purchased from Biolegend and/or
405 eBioscience™ and are listed in Supplementary Table 3.

406

407 To assess T_{RM} responses, intra-vascular labelling was performed as previously described[27].
408 Briefly, 3 µg anti-CD45.2 (104) conjugated to either FITC or APC was administered via i.v
409 injection into the tail vein in a final volume of 200 µl 3-5 minutes prior to performing
410 euthanasia. All flow cytometry data was analysed using FlowJo V10 software (Tree Star).

411

412 ***Tetramer Staining***

413 For assessment of Influenza virus-specific T cell responses, cells were transferred into 5 ml
414 round bottom polystyrene tubes, washed and incubated with Fc block for 15 minutes at room
415 temperature to prevent non-specific binding. Tetramers specific for $CD8^+$ T cells (H-2D(b)
416 Influenza A $NP_{366-374}$ (ASNENMETM) and H-2D(b) Influenza A $PA_{224-233}$ (SSLENFRAYV)) and $CD4^+$
417 cells (I-A(b) Influenza A $NP_{311-325}$ (QVYSLIRPNENPAHK)) recognising immunodominant
418 epitopes were obtained from the NIH tetramer facility at Emory University and added at 5
419 µg/ml in RPMI and incubated for a minimum of 1 hour at 37°C with regular agitation. Cells
420 were washed in PBS and staining performed as described below thereafter.

421

422

423

424 ***Quantitative PCR***

425 FACS-purified cells were sorted into complete media, washed in sterile PBS and re-suspended
426 in RLT buffer (Qiagen) containing 1% β-mercaptoethanol. For assessment of viral mRNA in
427 lung tissue a single lobe from the right lung was collected into a sterile 1.5 ml tube containing
428 RNA later and subsequently transferred into a 2ml tube containing RLT buffer and a single 2
429 mm stainless steel bead. Tissue was homogenised into suspension using a Qiagen Tissue
430 Lyser. RNA was extracted from both cells and lysed tissue samples using Qiagen RNeasy Mini
431 Kit as per manufacturer's instructions. Reverse transcription of RNA to cDNA was performed
432 using the High Capacity RNA-to-cDNA Kit (Thermo Fisher Scientific) and gene expression was
433 assayed using PowerUp™ SYBR™ Green Master Mix (Applied Biosystems). Reactions were run
434 on a real-time PCR system (ABI 7500; Applied Biosystems). Data for samples were normalized
435 to *Gapdh* and are shown as a fold change compared with the controls.

436 ***TGF-β Activation Assay***

437 FACS-purified T cell subsets were incubated overnight with a TGF-β reporter cell line[28] and
438 luciferase activity detected via the Luciferase Assay System (Promega). TGF-β activity was
439 determined as previously described[16].

440

441 ***RNA sequencing (RNA-seq)***

442 Total RNA was submitted to the Genomic Technologies Core Facility (GTCF) at the University
443 of Manchester and the quality and integrity of the RNA samples assessed using a 4200
444 TapeStation (Agilent Technologies) prior to the generation of libraries using the Illumina®
445 Stranded mRNA Prep. Ligation kit (Illumina, Inc.) according to the manufacturer's protocol.
446 Briefly, total RNA was used as input material from which polyadenylated mRNA was purified

447 using poly-T, oligo-attached, magnetic beads. Next, the mRNA was fragmented under
448 elevated temperature and then reverse transcribed into first strand cDNA using random
449 hexamer primers and in the presence of Actinomycin D (thus improving strand specificity
450 whilst mitigating spurious DNA-dependent synthesis). Following removal of the template
451 RNA, second strand cDNA was then synthesized to yield blunt-ended, double-stranded cDNA
452 fragments. Strand specificity was maintained by the incorporation of deoxyuridine
453 triphosphate (dUTP) in place of dTTP to quench the second strand during subsequent
454 amplification.

455 Following a single adenine (A) base addition, adapters with a corresponding, complementary
456 thymine (T) overhang were ligated to the cDNA fragments. Pre-index anchors were then
457 ligated to the ends of the double-stranded cDNA fragments to prepare them for dual indexing.
458 A subsequent PCR amplification step was then used to add the index adapter sequences to
459 create the final cDNA library. The adapter indices enabled the multiplexing of the libraries,
460 which were pooled prior to cluster generation using a cBot instrument. The loaded flow-cell
461 was then paired-end sequenced (76 + 76 cycles, plus indices) on an Illumina HiSeq4000
462 instrument. Finally, the output data was demultiplexed and BCL-to-Fastq conversion
463 performed using Illumina's bcl2fastq software (v2.20.0.422).

464

465 ***RNA-seq data analysis***

466 The quality of the stranded paired-end RNA-seq reads were assessed using FastQC (v0.11.3;
467 https://www.bioinformatics.babraham.ac.uk/projects/fastqc/) and FastQ Screen (v0.13.0;
468 https://www.bioinformatics.babraham.ac.uk/projects/fastq_screen/), followed by adapter
469 removal and low-quality bases and reads trimming using BBDuk (BBMap suite v36.32;

470 http://sourceforge.net/projects/bbmap/). Processed reads were mapped against the mouse
471 reference genome (mm10) and gene annotation from Gencode (vM24) using STAR (v2.7.2b;
472 https://doi.org/10.1093/bioinformatics/bts635). The "--quantMode GeneCounts" option was
473 used to obtain read counts per gene from STAR.
474 Differential gene expression analysis was performed in the R environment using the
475 Bioconductor package DESeq2 (v1.30.1; https://doi.org/10.1186/s13059-014-0550-8). Genes
476 were considered significantly differentially expressed with a false discovery rate cut-off of
477 0.05. The lfcShrink function (with apeglm method) was applied to produce a more accurate
478 log2 fold change estimates. The counts function (with normalized = TRUE) was used to
479 produce normalised counts, where it uses the median-of-ratios method to determine scaling
480 factors. Data transformation was performed using the rlog and vst functions to obtain
481 regularised logarithm and variance stabilizing transformation expression values respectively.
482 rlog transformed values were used to produce principal component analysis plots using the
483 prcomp function from the R package stats. vst values were used to produce sample-to-sample
484 correlation using the cor function from the R package stats. Heatmaps and correlation plots
485 were visualised using the R package pheatmap (v1.0.12).

486

487 ***T cell co-culture assays***

488 Spleens from *Itgb8*-IRES-TdTomato mice were manually dissociated, filtered through 40 µm
489 cell strainers and T cells enriched by negative selection using an EasySep™ pan-T cell
490 enrichment kit (Stemcell Technologies) as per manufacturer's guidelines. Splenic $CD4^+$ T_{EM}
491 and responder $CD8^+$ T cells from *Itgb8*-IRES-TdTomato mice were stained with cell surface
492 markers and further purified by FACS using a BD FACSAria™. $CD8^+$ T cells were subsequently

493 stained with CellTrace™ Violet proliferation dye (Thermo Fisher Scientific) and plated in a 1:1
494 ratio with *Itgb8*$^{+}$ or *Itgb8*$^{-}$ CD4^{+} T_{EM} in RPMI containing 0.88 mM L-Glutamine (Gibco), 0.88
495 mM sodium pyruvate (Gibco), 0.04 mM β-mercaptoethanol, 0.88% (v/v) MEM non-essential
496 amino acids (Gibco), 0.35% (v/v) 100X MEM Vitamins (Gibco), 4.4 U/ml penicillin (Gibco), 4.4
497 µg/ml streptomycin (Gibco) and 10% (v/v) heat-inactivated fetal calf serum (FCS) (Sigma).
498 Cells were added to sterile 96 well U-bottom tissue culture plates pre-coated with purified
499 NA/LE anti-CD3 (Clone 145-2C11) and soluble NA/LE anti-CD28 (Clone 37.51; both BD
500 Biosciences) added to provide co-stimulation. CD8^{+} T cell proliferative responses were
501 measured after 72 hours by assessing dye dilution across cell divisions on a BD Symphony™.

502

503 ***Adoptive transfer studies***

504 For adoptive transfer studies, *Itgb8*$^{+}$ or *Itgb8*$^{-}$ CD4^{+} T_{EM} were FACS-purified from the spleens
505 of convalescent *Itgb8*-IRES-TdTomato mice and 2 x 10^{5} of either cell type administered i.v into
506 the tail vein of IAV-X31 convalescent control or *Itgb8*$^{\Delta CD4}$ mice 1 day prior to re-challenge with
507 IAV-PR8.

508

509 ***Histological Assessment of Inflammation***

510 Mice were euthanised via intra-peritoneal injection of pentobarbitone and the thoracic cavity
511 opened to expose the lungs and trachea. The right lobes of the lungs were tied off and
512 removed for assessment of immune cell populations by flow cytometry. The remaining left
513 lobe was subsequently perfused with ~10 ml 1 mM EDTA in ice-cold PBS to remove
514 blood/circulating cells. The internal structure of the left lobe was then fixed by inflating with
515 1 ml 10% formalin via the trachea and the entire lobe subsequently immersed in 10% formalin

516 prior to transfer into 70% ethanol after 24 hours. Fixed lungs were embedded in paraffin and
517 sliced into 5 µm sections prior to staining with hematoxylin and eosin. Histopathology was
518 scored at 10x magnification of a light microscope according to a set of custom-designed
519 criteria to assess inflammation around airways, blood vessels and parenchyma as previously
520 described[29,30]. Six individual snapshots of each tissue section were analysed in a blinded
521 manner by two independent researchers and results collated.

522

523 ***Statistical Analysis***

524 Results are expressed as mean ± SEM. All statistical analysis was performed using GraphPad
525 Prism software (v9.4.1) and tests used are stated in the figure legends.

526

527

528

529

530

531

532

533

534

535

536

537

538

539 **Figure Legends:**

540 **Fig. 1| CD4$^+$ T$_{EM}$ activate latent TGFβ via integrin αvβ8 and possess an immune suppressive**
541 **transcriptional profile.** a) Expression of *Itgb8* in FACS-purified murine splenic T cell subsets as
542 determined by RT-PCR (n=≥6). Statistical significance determined by one-way ANOVA with
543 Tukey's multiple comparisons ****p=≤0.0001, ns = not significant. b) Representative flow
544 cytometry plots of *Itgb8* expression in splenic CD4$^+$ (black) and CD8$^+$ (grey) T cell subsets from
545 *Itgb8*-reporter mice. c) Collated data of *Itgb8* expression on CD4$^+$ and CD8$^+$ splenic T cells at
546 steady state. Data presented as frequency of *Itgb8*$^+$ cells as a percentage of each parent
547 population (n=8). Statistical significance determined by two-way ANOVA with Tukey's
548 multiple comparisons test ****p=≤0.0001, ns = not significant. d) Activation of latent TGFβ
549 by T$_{REG}$ (n=3, Foxp3-YFP$^+$) or CD4$^+$ T$_{EM}$ (n=6, CD44^{hi} CD62L^{lo} Foxp3$^-$) sorted from the spleen
550 of Foxp3^{YFP} mice or mice with a conditional deletion of *Itgb8* on T cells (*Itgb8*$^{\Delta CD4}$). Luciferase
551 activity detected following overnight co-culture of each T cell subset with a TGFβ responsive
552 reporter cell line. Data from two independent experiments. Statistical significance
553 determined by Kruskall-Wallis with Dunn's multiple comparisons test *p=≤0.05, ns = not
554 significant. e) Volcano plot of relative expression from bulk RNA-seq (n=6) between *Itgb8*$^-$ T$_{EM}$
555 (left) and *Itgb8*$^+$ T$_{EM}$ (right), with differential (Log$_2$ fold change > 0.5), statistically significant
556 genes (adjusted p < 0.05) indicated in red. f) Condensed heatmap of immune suppressive
557 genes differentially expressed between *Itgb8*$^+$ and *Itgb8*$^-$ T$_{EM}$ from bulk RNA-seq analysis
558 (n=6). g) PCA of bulk RNA-seq experiment performed on flow cytometry-purified splenic
559 CD44^{hi} CD62L^{lo} Foxp3$^+$ T$_{REG}$ (*Itgb8*$^+$ versus *Itgb8*$^-$) and CD44^{hi} CD62L^{lo} Foxp3$^-$ T$_{EM}$ (*Itgb8*$^+$ versus
560 *Itgb8*$^-$) (n = 3). h) Condensed heatmap of immune suppressive genes differentially expressed
561 between CD4$^+$ *Itgb8*$^+$ and *Itgb8*$^-$ T$_{EM}$ and T$_{REG}$ (n = 3).

562

563 **Fig. 2| Conditional deletion of *Itgb8* on CD4$^+$ T$_{EM}$ enhances Influenza virus-specific CD8$^+$ T**
564 **cell responses following heterologous secondary challenge.** a) Schematic of heterologous
565 secondary Influenza A Virus challenge protocol. Littermate control and *Itgb8*$^{\Delta CD4}$ mice were
566 infected with 10^3 PFU IAV-X31 resulting in a transient, self-resolving infection. Six weeks later,
567 mice were re-challenged with 10^1 PFU of the heterologous virus IAV-PR8 to facilitate
568 assessment of IAV-specific T cell responses. b) Representative flow plots of CD44^{hi} Influenza
569 nucleoprotein (NP$_{[366-374]}$)-specific CD8$^+$ T cells in the lungs of littermate control and *Itgb8*$^{\Delta CD4}$
570 mice 8 days following secondary infection with IAV-PR8 as determined by tetramer staining
571 (see Figure S3a for gating strategy). Frequencies shown are a percentage of total, live CD45$^+$,
572 single cells. c) Frequency and d) total number of NP-specific CD8$^+$ T cells in the lungs of
573 littermate control and *Itgb8*$^{\Delta CD4}$ mice at indicated time-points following re-challenge with IAV-
574 PR8. Data (n=3-10 biological replicates) from three independent experiments. Statistical
575 significance determined by two-way ANOVA with Tukey's multiple comparisons test
576 ***p=≤0.001, *p=≤0.05, ns = not significant. e) Representative flow plots of total CD8$^+$ T cells
577 producing Granzyme B in the lungs of littermate control and *Itgb8*$^{\Delta CD4}$ mice 5 days following
578 secondary infection with IAV-PR8 as determined by tetramer and intracellular staining. f)
579 Frequency (as a percentage of total live CD45$^+$ cells) and g) number of Granzyme B-producing
580 NP-specific CD8$^+$ T cells in the lungs of littermate control and *Itgb8*$^{\Delta CD4}$ mice 5 days following
581 secondary infection with IAV-PR8 (n=8 biological replicates). Statistical significance
582 determined by Mann-Whitney test **p=≤0.01, *p=≤0.05. h-k) 1 x 10^5 NP-specific CD8$^+$ T cells
583 were FACS-purified from the lungs of littermate control and *Itgb8*$^{\Delta CD4}$ mice 5 days following
584 secondary infection with IAV-PR8 and expression of h) *Gzma*, i) *Gzmb*, j) *Prf1* and k) *Ifng*
585 determined by RT-PCR (n=6 biological replicates from two independent experiments).
586 Statistical significance determined by Mann-Whitney test **p=≤0.01, *p=≤0.05.

587 **Fig. 3| *Itgb8*$^{+}$ CD4^{+} T$_{EM}$ restrain anti-viral CD8^{+} T cell responses following secondary**
588 **challenge and prevent CD8^{+} T cell proliferation via TGFβ.** a) Schematic of CD4^{+} T$_{EM}$ adoptive
589 transfer study. Littermate control, *Itgb8*$^{\Delta CD4}$ and *Itgb8*-reporter mice were infected with 10^3
590 PFU IAV-X31. 6 weeks post-infection, *Itgb8*$^{+}$ and *Itgb8*$^{-}$ CD4^{+} T$_{EM}$ were purified by flow
591 cytometry from convalescent *Itgb8*-reporter mice and transferred intravenously into
592 convalescent *Itgb8*$^{\Delta CD4}$ recipients, 24 hours prior to heterologous re-challenge with 10^1 PFU
593 IAV-PR8. b) Representative plots of NP-specific CD8^{+} T cells in the lungs of littermate control
594 and *Itgb8*$^{\Delta CD4}$ mice at day 8 post re-infection with IAV-PR8, the latter separated into two
595 cohorts based on having received either CD4^{+} *Itgb8*$^{+}$ or *Itgb8*$^{-}$ T$_{EM}$. c) Frequency, as a
596 percentage of total live CD45^{+} cells, of NP-specific CD8^{+} T cells in the lungs of littermate
597 control and *Itgb8*$^{\Delta CD4}$ mice receiving either CD4^{+} *Itgb8*$^{-}$ or *Itgb8*$^{+}$ T$_{EM}$ at day 8 post re-infection
598 with IAV-PR8. Data (n=≥9) from three independent experiments. Statistical significance
599 determined by Kruskall-Wallis with Dunn's multiple comparisons test **p=≤0.01, ns = not
600 significant. d) Representative histograms of Cell Tracer Violet-labelled naïve CD8^{+} T cell,
601 stimulated with anti-CD3 and anti-CD28 antibodies and co-cultured in a 1:1 ratio with *Itgb8*$^{+}$
602 or *Itgb8*$^{-}$ CD4^{+} T$_{EM}$ for 72 hours. Grey peaks represent CD8^{+} T cells co-cultured with *Itgb8*$^{-}$ CD4^{+}
603 T$_{EM}$, purple peaks signify CD8^{+} T cells co-cultured with *Itgb8*$^{+}$ CD4^{+} T$_{EM}$ and green peaks
604 represent CD8^{+} T cells co-cultured with *Itgb8*$^{+}$ CD4^{+} T$_{EM}$ in the presence of a TGFβ blocking
605 antibody. e) Pooled data for frequency of CD8^{+} T cells undergoing proliferation under each
606 condition in d (n=5 biological replicates from two independent experiments). Statistical
607 significance determined by one-way ANOVA with Tukey's multiple comparisons test
608 ***p=≤0.001, **p=≤0.01, ns = not significant. f) Representative histograms and g) collated
609 data of naïve CD8^{+} T cell proliferative responses following co-culture in a 1:1 ratio with *Itgb8*$^{-}$
610 CD4^{+} T$_{EM}$ plus or minus recombinant TGFβ for 72 hours. Grey peaks/dots represent CD8^{+} T

611 cells co-cultured with *Itgb8*$^{-}$ CD4^{+} $T_{EM,}$ blue plots/dots represent CD8^{+} T cells co-cultured 1:1
612 with *Itgb8*$^{-}$ CD4^{+} T_{EM} in the presence of recombinant TGFβ (n=5 biological replicates from two
613 independent experiments). Statistical significance determined by unpaired student's t-test
614 ****p=≤0.0001.
615
616 **Fig. 4| Conditional deletion of *Itgb8* on CD4^{+} T_{EM} facilitates rapid viral clearance but induces**
617 **significant tissue pathology.** a) Viral Matrix (M) protein mRNA in the lungs of littermate
618 control and *Itgb8*$^{\Delta CD4}$ mice at indicated time-points following re-challenge with IAV-PR8 as
619 determined by RT-PCR (n=≥4 biological replicates per-timepoint from two independent
620 experiments). Statistical significance determined by two-way ANOVA with Šídák's multiple
621 comparisons test ****p=≤0.0001. b) Representative images of H&E-stained lung tissue
622 sections from littermate control and *Itgb8*$^{\Delta CD4}$ mice 8 days following re-challenge with IAV-
623 PR8. c) Inflammation scores of blind-scored H&E-stained lung tissue sections from littermate
624 control and *Itgb8*$^{\Delta CD4}$ mice 8 days following re-challenge with IAV-PR8 (n=6 biological
625 replicates). Statistical significance determined by Mann-Whitney test **p=≤0.01. d)
626 Representative images of H&E-stained lung tissue sections from *Itgb8*$^{\Delta CD4}$ mice 8 days
627 following re-challenge with IAV-PR8. 24 hours prior to re-challenge, *Itgb8*$^{\Delta CD4}$ mice were
628 adoptively transferred with either *Itgb8*$^{-}$ CD4^{+} T_{EM} (grey) or *Itgb8*$^{+}$ CD4^{+} T_{EM} (purple) purified
629 from convalescent *Itgb8*-reporter mice. e) Inflammation scores of blind-scored H&E-stained
630 lung tissue sections from *Itgb8*$^{\Delta CD4}$ recipient mice 8 days following re-challenge with IAV-PR8.
631 Statistical significance determined by Mann-Whitney test **p=≤0.01. f) Frequency of integrin
632 αvβ8-expressing cells amongst CD4^{+} and CD8^{+} T cell subsets in human PBMCs. Frequencies
633 shown are a percentage of total CD3^{+} cells (n=10 individual donors). Statistical significance
634 determined by two-way ANOVA with Tukey's multiple comparisons test. g) Pairwise

635 comparison of integrin αvβ8-expressing $CD4^+$ and $CD8^+$ T_{EM} in human PBMCs. Statistical

636 significance determined by two-tailed, paired student's t-test ****p=≤0.0001.

637

638

639

640

641

642

643

644

645

646

647

648

649

650

651

652

653

654

655

656

657

658

659 **Supplementary Figure Legends**

660

661 **Fig. S1| *Itgb8*-expressing CD4$^+$ T_{EM} are present in non-lymphoid tissues.** a) Representative
662 gating strategy for analysing and sorting murine splenic T cell subsets. b) Representative flow
663 plots and c) collated data showing *Itgb8* expression in lung CD4$^+$ T cell subsets of *Itgb8*-
664 reporter mice. d) Representative flow plots and c) collated data showing *Itgb8* expression in
665 small intestinal CD4$^+$ T cell subsets of *Itgb8*-reporter mice. Data presented as frequency of
666 *Itgb8*$^+$ cells as a percentage of each parent population (n=3 biological replicates for each
667 tissue, representative of two independent experiments). Statistical significance determined
668 by two-way ANOVA with Tukey's multiple comparisons test ****p=≤0.0001, ns = not
669 significant.

670

671 **Fig. S2| *Itgb8*-expressing CD4$^+$ T_{EM} and T_{REG} possess a characteristic immune suppressive**
672 **transcriptional profile.** a) Heatmap of Z-scores of regularized variance stabilizing transformed
673 read counts from bulk RNA-seq (n=6) analysing CD4$^+$ *Itgb8*$^-$ T_{EM} (left, black) and CD4$^+$ *Itgb8*$^-$
674 T_{EM} (right, red), with differential (Log_2 fold change > 0.5), statistically significant (adjusted p <
675 0.05) genes indicated. b) Principal component analysis (PCA) of bulk RNA-seq experiment
676 performed on flow cytometry-purified splenic *Itgb8*$^+$ T_{EM} versus *Itgb8*$^-$ T_{EM} (n = 6). c) Sample
677 similarity heatmap showing Pearson correlation between samples calculated using
678 regularized logarithmic (rlog)-transformed read counts. d) Heatmap of Z-scores of regularized
679 variance stabilizing transformed read counts of selected genes associated with T cell biology.

680

681 **Fig. S3| Analysis of Influenza virus-specific T cell responses following primary and**
682 **heterologous secondary challenge in *Itgb8*$^{\Delta CD4}$ and *Itgb8*$^{\Delta Foxp3}$ mice.** a) Representative gating

683 strategy used to identify Influenza NP-specific $CD8^+$ T cells, as well as tissue-resident cells, in
684 the lung of mice. b) Representative flow plots and c) collated data for the frequency of $CD44^{hi}$
685 Influenza NP-specific $CD8^+$ T cells in the draining mediastinal lymph nodes of littermate
686 control and *Itgb8*$^{\Delta CD4}$ mice at indicated time-points post-secondary IAV-PR8 infection (n= ≥6
687 biological replicates from two independent experiments). Frequencies shown are as a
688 percentage of total $CD8^+$ T cells per node. Statistical significance determined by two-way
689 ANOVA with Tukey's multiple comparisons test **p=≤0.01. d) Representative flow plots and
690 e) collated data for the frequency of $CD44^{hi}$ Influenza NP-specific $CD4^+$ T cells in the lungs of
691 littermate control and *Itgb8*$^{\Delta CD4}$ mice at indicated time-points post re-challenge infection with
692 IAV-PR8 (n=≥4 biological replicates per timepoint, from three independent experiments).
693 Frequencies shown are as a percentage of total, live $CD45^+$, single cells per lung. Statistical
694 significance determined by two-way ANOVA with Tukey's multiple comparisons test. f)
695 Representative flow cytometry plots and g) collated data for the frequency of NP-specific
696 $CD8^+$ T cells in the lungs of littermate control and *Itgb8*$^{\Delta CD4}$ mice at indicated time-points post
697 primary infection with IAV-PR8 (n=≥3 biological replicates per timepoint representative of
698 three independent experiments). Statistical significance determined by two-way ANOVA with
699 Tukey's multiple comparisons test. h) Representative flow cytometry plots and i) collated data
700 for the frequency of $CD44^{hi}$ Influenza NP-specific $CD8^+$ T cells in the lungs of littermate control
701 and *Itgb8*$^{\Delta Foxp3}$ mice at indicated time-points following secondary infection with IAV-PR8
702 (n=10 biological replicates from two independent experiments, n=3 for day 0 controls).
703 Statistical significance determined by two-way ANOVA with Tukey's multiple comparisons
704 test. j) Representative flow cytometry plots and k) collated data for frequency of Granzyme
705 B-producing NP-specific $CD8^+$ T cells in the mediastinal lymph nodes of littermate control and
706 *Itgb8*$^{\Delta CD4}$ mice at indicated time-points post-secondary infection with IAV-PR8. Statistical

707 significance determined by two-way ANOVA with Tukey's multiple comparisons test
708 **p=≤0.01. (n=≥4 biological replicates from two independent experiments). Frequencies
709 shown are as a percentage of total $CD8^+$ T cells per node. l) Frequency of intra-vascular
710 (CD45.2 I.V+) and extra-vasculature (CD45.2-) NP-specific $CD8^+$ T cells in the lungs of
711 littermate control and *Itgb8*$^{\Delta CD4}$ mice 8 days following secondary infection with IAV-PR8, as
712 determined by intra-vascular labelling and tetramer staining (n=5 biological replicates from
713 two independent experiments). Statistical significance determined by two-way ANOVA with
714 Tukey's multiple comparisons test ****p=≤0.0001, *p=≤0.05.
715
716 **Fig. S4| *Itgb8*$^+$ CD4$^+$ T_{EM} restrain anti-IAV PA-specific CD8$^+$ T cell responses following**
717 **secondary challenge.** a) Representative flow cytometry plots of viral polymerase ($PA_{[224-233]}$)-
718 specific $CD8^+$ T cells in the lungs of littermate control and *Itgb8*$^{\Delta CD4}$ mice at day 8 post re-
719 infection with IAV-PR8, the latter separated into two cohorts on the basis of having received
720 *Itgb8*$^+$ or *Itgb8*$^-$ CD4$^+$ T_{EM} intravenously one day prior to re-challenge. b) Frequency, as a
721 percentage of total, live $CD45^+$ single cells, of PA-specific $CD8^+$ T cells in the lungs of littermate
722 control and both cohorts of *Itgb8*$^{\Delta CD4}$ mice at day 8 post re-infection with IAV-PR8 (n=≥9
723 biological replicates from three independent experiments). Statistical significance
724 determined by Kruskall-Wallis with Dunn's multiple comparisons test *p=≤0.05, ns = not
725 significant.
726
727 **Fig. S5| Expression of *Itgb8*$^+$ on Foxp3$^+$ T_{reg} does not control viral titre and *Itgb8*$^+$ CD4$^+$ T_{EM}**
728 **do not control lung pathology following primary IAV challenge.** a) Viral Matrix (M) protein
729 mRNA in the lungs of littermate control and *Itgb8*$^{\Delta Foxp3}$ mice at indicated time-points following
730 heterologous re-challenge with IAV-PR8 as determined by RT-PCR (n=3-5 biological replicates

731 per-timepoint). Statistical significance determined by two-way ANOVA with Tukey's multiple
732 comparisons test. b) Representative images of H&E-stained lung tissue sections from
733 littermate control and *Itgb8*$^{\Delta CD4}$ mice 6 weeks following primary infection with IAV-PR8. c)
734 Inflammation scores of blind-scored H&E-stained lung tissue sections from littermate control
735 and *Itgb8*$^{\Delta CD4}$ mice 6 weeks following primary infection with IAV-PR8 (n=4 biological
736 replicates). Statistical significance determined by Mann-Whitney test.
737
738 **Fig. S6| Gating strategy for assessment of integrin αvβ8 expression of human T cell subsets.**
739 Representative gating strategy used to identify naïve T cells, T_{CM}, T_{EM} and T_{EMRA} in human
740 PBMC samples isolated from whole blood by Ficoll density gradient centrifugation.
741
742 **Table S1: Differentially expressed genes between *Itgb8*$^{+}$ and *Itgb8*$^{-}$ CD4^{+} T_{EM}.** List of 1599
743 differentially expressed protein-encoding genes between *Itgb8*$^{+}$ and *Itgb8*$^{-}$ CD4^{+} T_{EM} with a
744 Log_2 fold change greater than 0.5 and adjusted p-value of <0.05 (from RNA-seq experiment
745 shown in Figure 1e and Figure S2a-b).
746
747 **Table S2: Differentially expressed genes between *Itgb8*$^{+}$ and *Itgb8*$^{-}$ CD4+ T_{EM} and T_{REG}.** List
748 of differentially expressed protein-encoding genes from all possible two-way comparisons
749 between *Itgb8*$^{+}$ and *Itgb8*$^{-}$ CD4+ T_{EM} and T_{REG}, where a gene displayed a Log2 fold change
750 greater than 0.5 and adjusted p-value of <0.05 for any comparison (from RNA-seq experiment
751 shown in Figure 1g and Figure S2c-d).
752
753 **Table S3: List of flow cytometry antibodies and reagents used.**
754

755 **References.**

756 1 Altenburg, A. F., Rimmelzwaan, G. F. & de Vries, R. D. Virus-specific T cells as correlate of
757 (cross-)protective immunity against influenza. *Vaccine* **33**, 500-506 (2015).
758 https://doi.org:10.1016/j.vaccine.2014.11.054

759 2 Thomas, P. G., Keating, R., Hulse-Post, D. J. & Doherty, P. C. Cell-mediated protection in
760 influenza infection. *Emerg Infect Dis* **12**, 48-54 (2006).
761 https://doi.org:10.3201/eid1201.051237

762 3 Lees, J. R. & Farber, D. L. Generation, persistence and plasticity of CD4 T-cell memories.
763 *Immunology* **130**, 463-470 (2010). https://doi.org:10.1111/j.1365-2567.2010.03288.x

764 4 Omilusik, K. D. & Goldrath, A. W. Remembering to remember: T cell memory maintenance
765 and plasticity. *Curr Opin Immunol* **58**, 89-97 (2019). https://doi.org:10.1016/j.coi.2019.04.009

766 5 Jameson, S. C. & Masopust, D. Understanding Subset Diversity in T Cell Memory. *Immunity* **48**,
767 214-226 (2018). https://doi.org:10.1016/j.immuni.2018.02.010

768 6 Sasson, S. C., Gordon, C. L., Christo, S. N., Klenerman, P. & Mackay, L. K. Local heroes or villains:
769 tissue-resident memory T cells in human health and disease. *Cell Mol Immunol* **17**, 113-122
770 (2020). https://doi.org:10.1038/s41423-019-0359-1

771 7 Stolley, J. M. *et al.* Retrograde migration supplies resident memory T cells to lung-draining LN
772 after influenza infection. *J Exp Med* **217** (2020). https://doi.org:10.1084/jem.20192197

773 8 Kelly, A., Houston, S. A., Sherwood, E., Casulli, J. & Travis, M. A. Regulation of Innate and
774 Adaptive Immunity by TGFbeta. *Adv Immunol* **134**, 137-233 (2017).
775 https://doi.org:10.1016/bs.ai.2017.01.001

776 9 Robertson, I. B. & Rifkin, D. B. Regulation of the Bioavailability of TGF-beta and TGF-beta-
777 Related Proteins. *Cold Spring Harb Perspect Biol* **8** (2016).
778 https://doi.org:10.1101/cshperspect.a021907

779 10 McEntee, C. P., Gunaltay, S. & Travis, M. A. Regulation of barrier immunity and homeostasis
780 by integrin-mediated transforming growth factor beta activation. *Immunology* **160**, 139-148
781 (2020). https://doi.org:10.1111/imm.13162
782 11 Rubtsov, Y. P. *et al.* Regulatory T cell-derived interleukin-10 limits inflammation at
783 environmental interfaces. *Immunity* **28**, 546-558 (2008).
784 https://doi.org:10.1016/j.immuni.2008.02.017
785 12 Worthington, J. J. *et al.* Integrin alphavbeta8-Mediated TGF-beta Activation by Effector
786 Regulatory T Cells Is Essential for Suppression of T-Cell-Mediated Inflammation. *Immunity* **42**,
787 903-915 (2015). https://doi.org:10.1016/j.immuni.2015.04.012
788 13 Nakawesi, J. *et al.* alphavbeta8 integrin-expression by BATF3-dependent dendritic cells
789 facilitates early IgA responses to Rotavirus. *Mucosal Immunol* **14**, 53-67 (2021).
790 https://doi.org:10.1038/s41385-020-0276-8
791 14 Travis, M. A. *et al.* Loss of integrin alpha(v)beta8 on dendritic cells causes autoimmunity and
792 colitis in mice. *Nature* **449**, 361-365 (2007). https://doi.org:10.1038/nature06110
793 15 Fenton, T. M. *et al.* Inflammatory cues enhance TGFbeta activation by distinct subsets of
794 human intestinal dendritic cells via integrin alphavbeta8. *Mucosal Immunol* **10**, 624-634
795 (2017). https://doi.org:10.1038/mi.2016.94
796 16 Worthington, J. J., Czajkowska, B. I., Melton, A. C. & Travis, M. A. Intestinal dendritic cells
797 specialize to activate transforming growth factor-beta and induce Foxp3+ regulatory T cells
798 via integrin alphavbeta8. *Gastroenterology* **141**, 1802-1812 (2011).
799 https://doi.org:10.1053/j.gastro.2011.06.057
800 17 Lacy-Hulbert, A. *et al.* Ulcerative colitis and autoimmunity induced by loss of myeloid alphav
801 integrins. *Proc Natl Acad Sci U S A* **104**, 15823-15828 (2007).
802 https://doi.org:10.1073/pnas.0707421104

803 18 Paidassi, H. *et al.* Preferential expression of integrin alphavbeta8 promotes generation of
804 regulatory T cells by mouse CD103+ dendritic cells. *Gastroenterology* **141**, 1813-1820 (2011).
805 https://doi.org:10.1053/j.gastro.2011.06.076
806 19 Kelly, A. *et al.* Human monocytes and macrophages regulate immune tolerance via integrin
807 alphavbeta8-mediated TGFbeta activation. *J Exp Med* **215**, 2725-2736 (2018).
808 https://doi.org:10.1084/jem.20171491
809 20 Mohammed, J. *et al.* Stromal cells control the epithelial residence of DCs and memory T cells
810 by regulated activation of TGF-beta. *Nat Immunol* **17**, 414-421 (2016).
811 https://doi.org:10.1038/ni.3396
812 21 Hirai, T. *et al.* Keratinocyte-Mediated Activation of the Cytokine TGF-beta Maintains Skin
813 Recirculating Memory CD8(+) T Cells. *Immunity* **50**, 1249-1261 e1245 (2019).
814 https://doi.org:10.1016/j.immuni.2019.03.002
815 22 Mani, V. *et al.* Migratory DCs activate TGF-beta to precondition naive CD8(+) T cells for tissue-
816 resident memory fate. *Science* **366** (2019). https://doi.org:10.1126/science.aav5728
817 23 McKarns, S. C. & Schwartz, R. H. Distinct effects of TGF-beta 1 on CD4+ and CD8+ T cell survival,
818 division, and IL-2 production: a role for T cell intrinsic Smad3. *J Immunol* **174**, 2071-2083
819 (2005). https://doi.org:10.4049/jimmunol.174.4.2071
820 24 Laine, A. *et al.* Regulatory T cells promote cancer immune-escape through integrin
821 alphavbeta8-mediated TGF-beta activation. *Nat Commun* **12**, 6228 (2021).
822 https://doi.org:10.1038/s41467-021-26352-2
823 25 Dodagatta-Marri, E. *et al.* Integrin alphavbeta8 on T cells suppresses anti-tumor immunity in
824 multiple models and is a promising target for tumor immunotherapy. *Cell Rep* **36**, 109309
825 (2021). https://doi.org:10.1016/j.celrep.2021.109309
826 26 Takasaka, N. *et al.* Integrin alphavbeta8-expressing tumor cells evade host immunity by
827 regulating TGF-beta activation in immune cells. *JCI Insight* **3** (2018).
828 https://doi.org:10.1172/jci.insight.122591

829 27 Anderson, K. G. *et al.* Intravascular staining for discrimination of vascular and tissue
830 leukocytes. *Nat Protoc* **9**, 209-222 (2014). https://doi.org:10.1038/nprot.2014.005
831 28 Abe, M. *et al.* An assay for transforming growth factor-beta using cells transfected with a
832 plasminogen activator inhibitor-1 promoter-luciferase construct. *Anal Biochem* **216**, 276-284
833 (1994). https://doi.org:10.1006/abio.1994.1042
834 29 Liu, G. *et al.* Platelet activating factor receptor regulates colitis-induced pulmonary
835 inflammation through the NLRP3 inflammasome. *Mucosal Immunol* **12**, 862-873 (2019).
836 https://doi.org:10.1038/s41385-019-0163-3
837 30 Horvat, J. C. *et al.* Neonatal chlamydial infection induces mixed T-cell responses that drive
838 allergic airway disease. *Am J Respir Crit Care Med* **176**, 556-564 (2007).
839 https://doi.org:10.1164/rccm.200607-1005OC
840

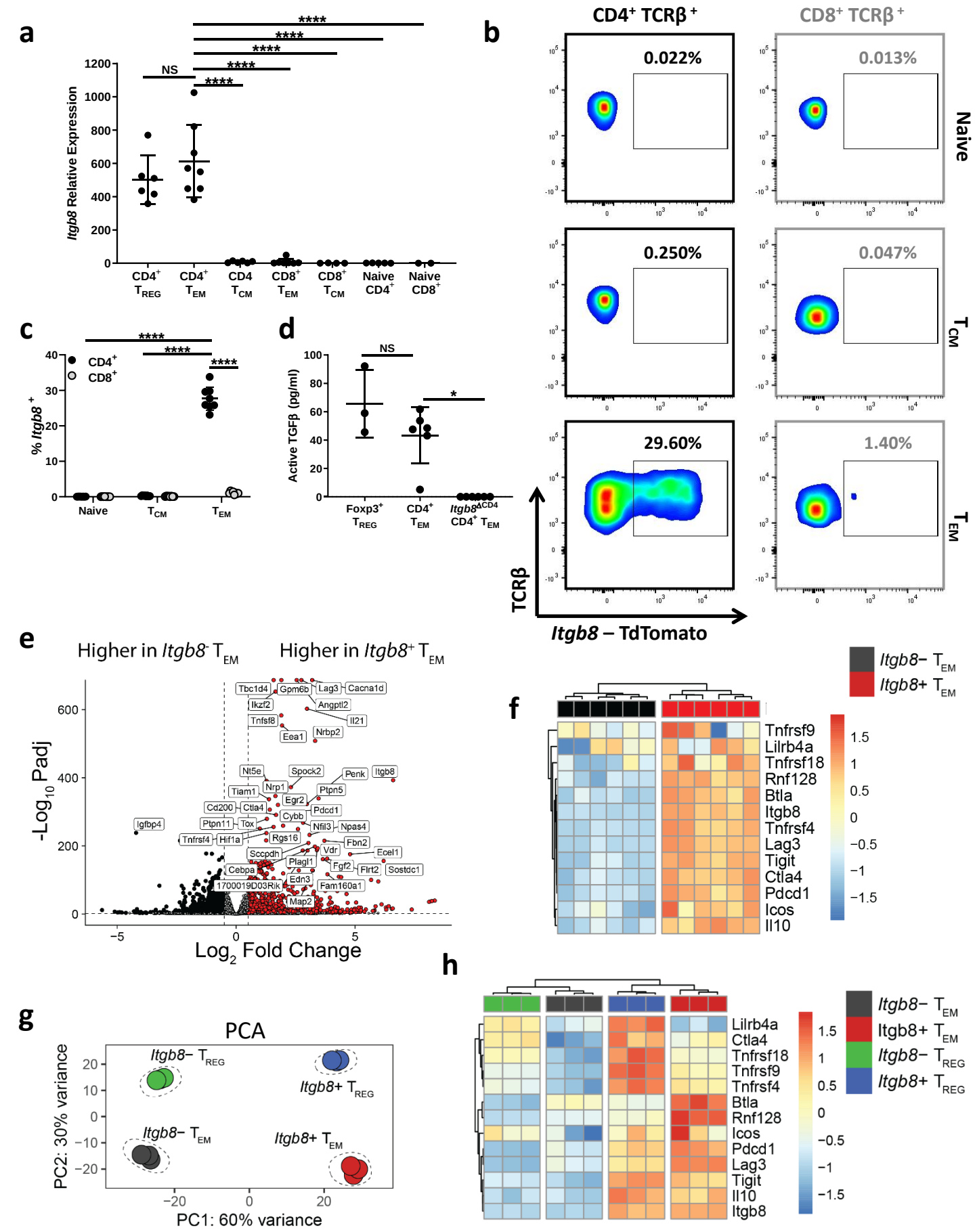
a
Itgb8 Relative Expression
NS
****
CD4+ TREG
CD4+ TEM
CD4 TCM
CD8+ TEM
CD8+ TCM
Naive CD4+
Naive CD8+
b
CD4+ TCRβ+
CD8+ TCRβ+
0.022%
0.013%
Naive
0.250%
0.047%
TCM
29.60%
1.40%
TEM
TCRβ
Itgb8 – TdTomato
c
% Itgb8+
CD4+
CD8+
Naive
TCM
TEM
d
Active TGFβ (pg/ml)
NS
*
Foxp3+ TREG
CD4+ TEM
Itgb8ΔCD4 CD4+ TEM
e
Higher in Itgb8- TEM
Higher in Itgb8+ TEM
-Log10 Padj
Log2 Fold Change
Tbc1d4
Gpm6b
Lag3
Cacna1d
Ikzf2
Angptl2
Tnfsf8
Il21
Eea1
Nrbp2
Nt5e
Spock2
Penk
Itgb8
Tiam1
Nrp1
Ptpn5
Egr2
Cd200
Ctla4
Pdcd1
Cybb
Igfbp4
Ptpn11
Tox
Nfil3
Npas4
Tnfrsf4
Hif1a
Rgs16
Fbn2
Vdr
Ecel1
Sccpdh
Plagl1
Fgf2
Flrt2
Sostdc1
Cebpa
Edn3
1700019D03Rik
Fam160a1
Map2
f
Itgb8− TEM
Itgb8+ TEM
Tnfrsf9
Lilrb4a
Tnfrsf18
Rnf128
Btla
Itgb8
Tnfrsf4
Lag3
Tigit
Ctla4
Pdcd1
Icos
Il10
g
PCA
Itgb8− TREG
Itgb8+ TREG
Itgb8− TEM
Itgb8+ TEM
PC2: 30% variance
PC1: 60% variance
h
Itgb8− TEM
Itgb8+ TEM
Itgb8− TREG
Itgb8+ TREG
Lilrb4a
Ctla4
Tnfrsf18
Tnfrsf9
Tnfrsf4
Btla
Rnf128
Icos
Pdcd1
Lag3
Tigit
Il10
Itgb8

Figure 1

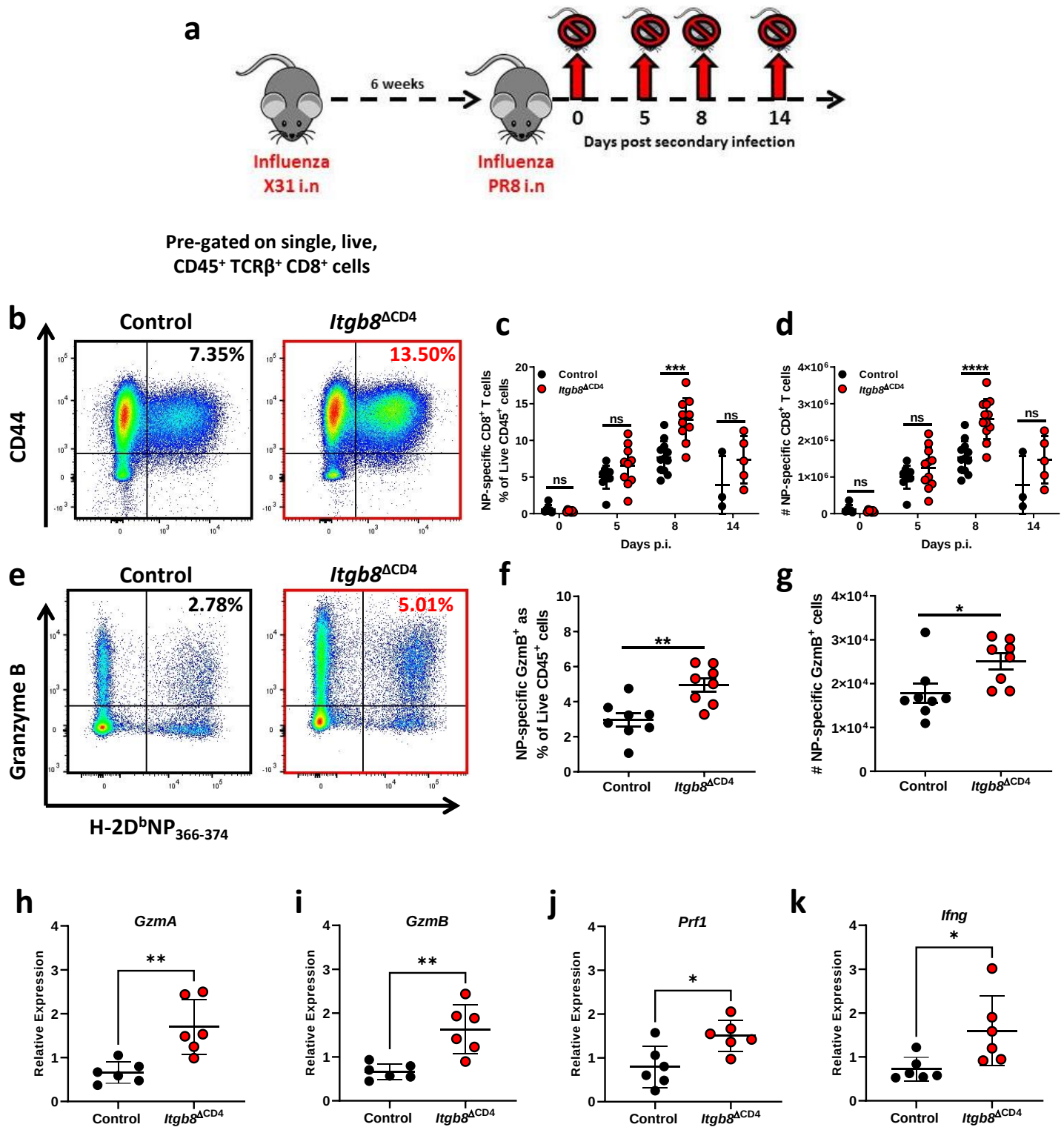
a
6 weeks
Influenza X31 i.n
Influenza PR8 i.n
0
5
8
14
Days post secondary infection
Pre-gated on single, live, CD45+ TCRβ+ CD8+ cells
b
Control
Itgb8ΔCD4
7.35%
13.50%
CD44
c
NP-specific CD8+ T cells % of Live CD45+ cells
Control
Itgb8ΔCD4
ns
***
Days p.i.
d
NP-specific CD8+ T cells
****
e
2.78%
5.01%
Granzyme B
H-2DbNP366-374
f
NP-specific GzmB+ as % of Live CD45+ cells
**
g
NP-specific GzmB+ cells
*
h
GzmA
Relative Expression
i
GzmB
j
Prf1
k
Ifng

Figure 2

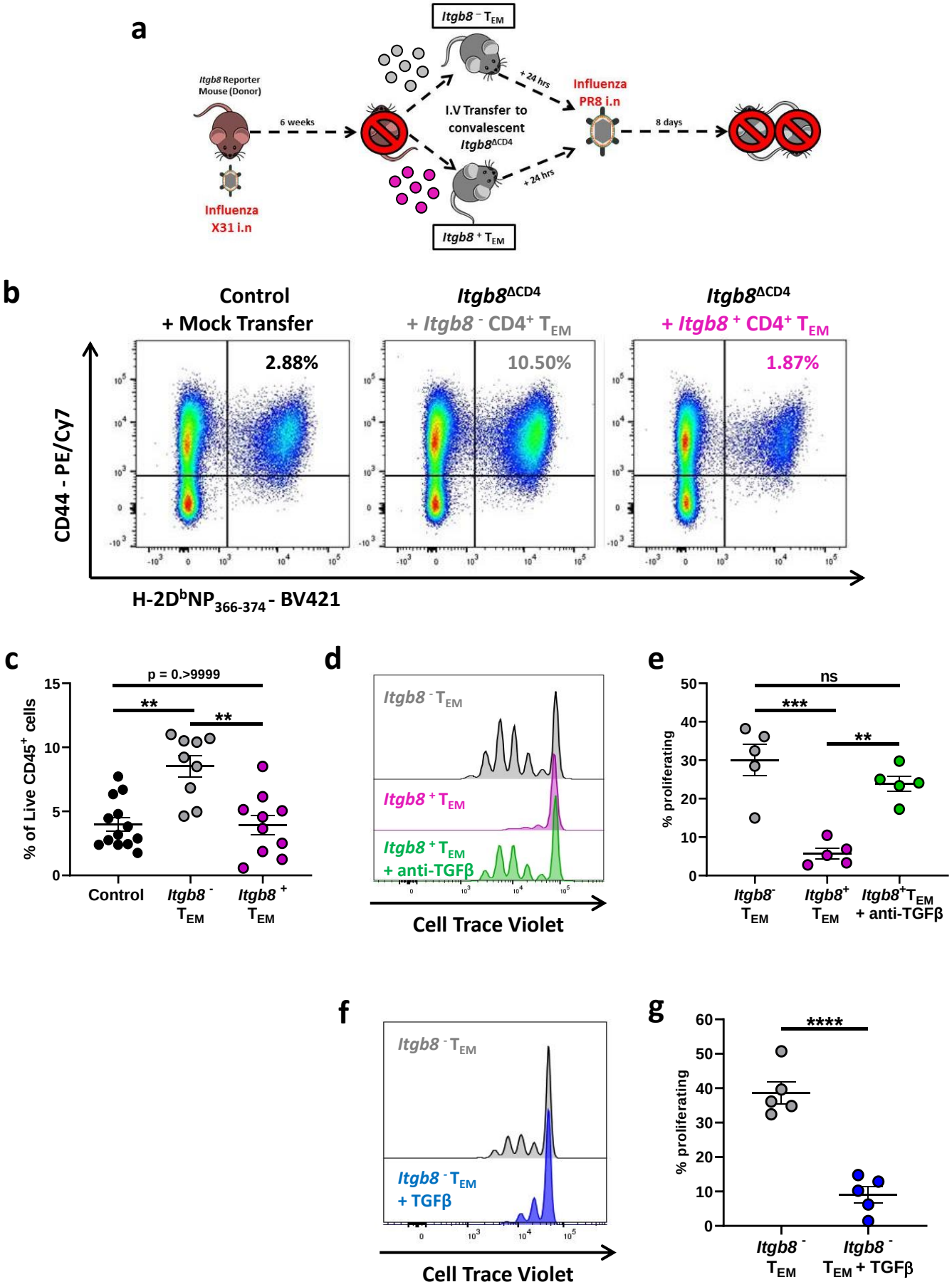
a
Itgb8 Reporter Mouse (Donor)
6 weeks
Influenza X31 i.n
Itgb8 - TEM
Itgb8 + TEM
I.V Transfer to convalescent Itgb8ΔCD4
+ 24 hrs
+ 24 hrs
Influenza PR8 i.n
8 days
b
Control + Mock Transfer
Itgb8ΔCD4 + Itgb8 - CD4+ TEM
Itgb8ΔCD4 + Itgb8 + CD4+ TEM
2.88%
10.50%
1.87%
CD44 - PE/Cy7
H-2DbNP366-374 - BV421
c
p = 0.>9999
**
**
% of Live CD45+ cells
Control
Itgb8 - TEM
Itgb8 + TEM
d
Itgb8 - TEM
Itgb8 + TEM
Itgb8 + TEM + anti-TGFβ
Cell Trace Violet
e
ns
***
**
% proliferating
Itgb8- TEM
Itgb8+ TEM
Itgb8+TEM + anti-TGFβ
f
Itgb8 - TEM
Itgb8 - TEM + TGFβ
Cell Trace Violet
g
****
% proliferating
Itgb8 - TEM
Itgb8 - TEM + TGFβ

Figure 3

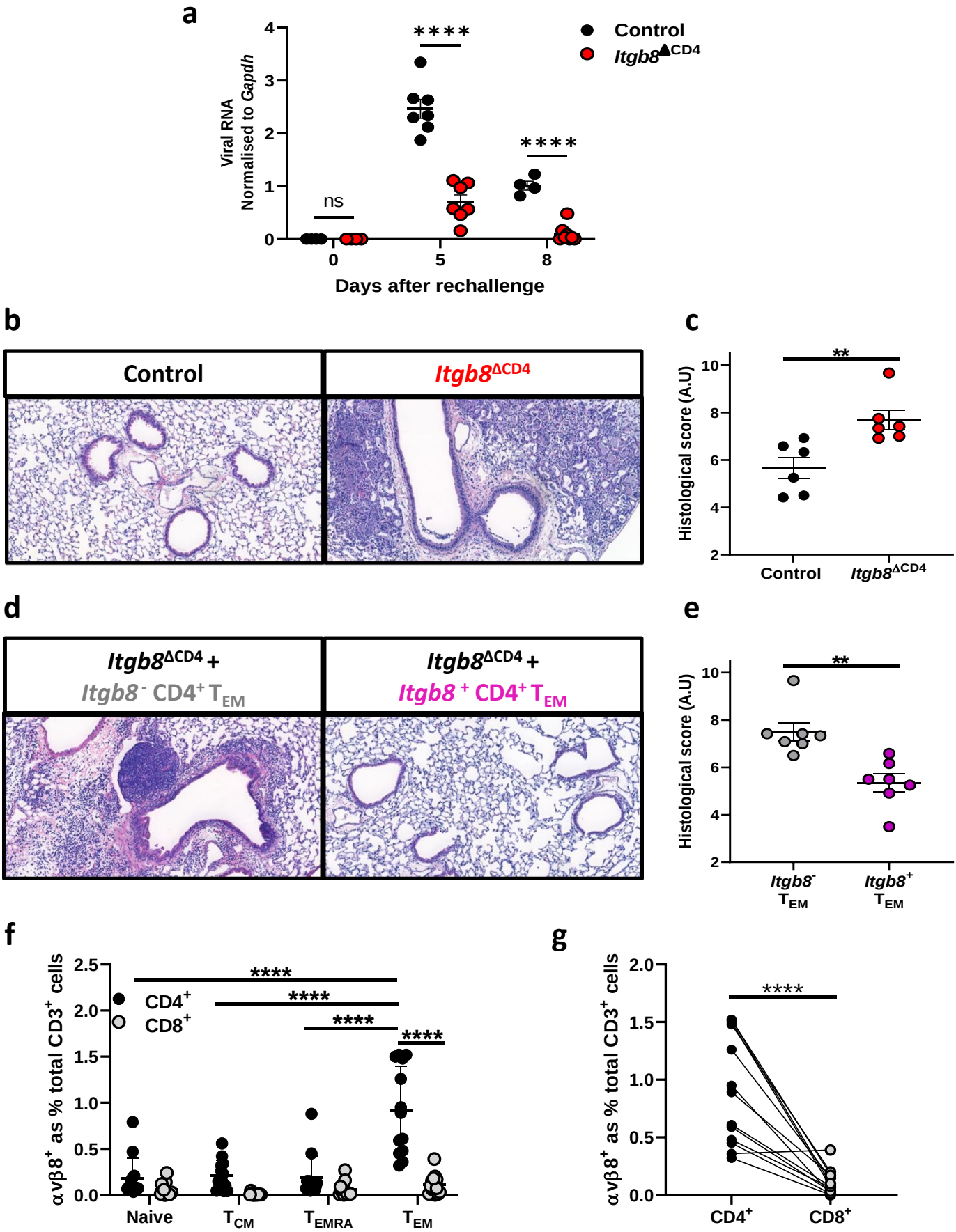
a
Viral RNA Normalised to Gapdh
Days after rechallenge
Control
Itgb8ΔCD4
ns
****
****
b
Control
Itgb8ΔCD4
c
Histological score (A.U)
Control
Itgb8ΔCD4
**
d
Itgb8ΔCD4 +
Itgb8- CD4+ TEM
Itgb8ΔCD4 +
Itgb8 + CD4+ TEM
e
Histological score (A.U)
Itgb8- TEM
Itgb8+ TEM
**
f
αvβ8+ as % total CD3+ cells
CD4+
CD8+
Naive
TCM
TEMRA
TEM
****
g
αvβ8+ as % total CD3+ cells
CD4+
CD8+
****

Figure 4